JBC RESEARCH ARTICLE

Nucleolin acts as the receptor for C1QTNF4 and supports C1QTNF4-mediated innate immunity modulation

Received for publication, November 10, 2020, and in revised form, February 26, 2021 Published, Papers in Press, March 4, 2021,
https://doi.org/10.1016/j.jbc.2021.100513

Susan K. Vester[1], Rebecca L. Beavil[2,3], Steven Lynham[4], Andrew J. Beavil[2,3], Deborah S. Cunninghame Graham[1], James M. McDonnell[2,3], and Timothy J. Vyse[1,*]

From the [1]Department of Medical & Molecular Genetics, [2]Randall Centre for Cell and Molecular Biophysics, King's College London, London, UK; [3]Asthma UK Centre in Allergic Mechanisms of Asthma, London, UK; [4]Proteomics Facility, Centre of Excellence for Mass Spectrometry, King's College London, London, UK

Edited by Peter Cresswell

The C1q and TNF related 4 (C1QTNF4) protein is a structurally unique member of the C1QTNF family, a family of secreted proteins that have structural homology with both complement C1q and the tumor necrosis factor superfamily. C1QTNF4 has been linked to the autoimmune disease systemic lupus erythematosus through genetic studies; however, its role in immunity and inflammation remains poorly defined and a cell surface receptor of C1QTNF4 has yet to be identified. Here we report identification of nucleolin as a cell surface receptor of C1QTNF4 using mass spectrometric analysis. Additionally, we present evidence that the interaction between C1QTNF4 and nucleolin is mediated by the second C1q-like domain of C1QTNF4 and the C terminus of nucleolin. We show that monocytes and B cells are target cells of C1QTNF4 and observe extensive binding to dead cells. Imaging flow cytometry experiments in monocytes show that C1QTNF4 becomes actively internalized upon cell binding. Our results suggest that nucleolin may serve as a docking molecule for C1QTNF4 and act in a context-dependent manner through coreceptors. Taken together, these findings further our understanding of C1QTNF4's function in the healthy immune system and how dysfunction may contribute to the development of systemic lupus erythematosus.

C1q and tumor necrosis factor (TNF) related 4 (C1QTNF4) is a member of the C1q and TNF related (C1QTNF) family, a family of secreted proteins that were initially identified as paralogs of adiponectin (1) and have structural homology with both complement C1q and the TNF superfamily (2). C1QTNF4 is structurally unique, comprising two C1q-like domains connected by a short linker and lacking a collagen-like region. C1QTNF4's functions remain poorly understood, with studies suggesting roles in cancer-related inflammation (3, 4), virus-related inflammation (5), as well as metabolism and food intake (6–8). To date, a receptor of C1QTNF4 has not been identified and there are conflicting reports of function; proinflammatory properties of C1QTNF4 have been reported *in vitro* (3), while anti-inflammatory properties have been observed *in vivo* (4). While both studies provide some indication that C1QTNF4 may be involved in signaling pathways upstream of interleukin 6 (IL-6), the molecular mechanisms underlying many of C1QTNF4's reported functions remain unknown.

Systemic lupus erythematosus (SLE) is an autoimmune inflammatory disease of complex genetic etiology that involves both the innate and adaptive immune system. Genetic advances have implicated many pathogenic pathways, including immune complex and waste clearance, interferon and toll-like receptor (TLR) signaling, as well as aberrant lymphocyte activation (9). A rare novel *de novo* mutation in *C1QTNF4*, a histidine to glutamine missense variant (H198Q), was recently discovered through exome sequencing of SLE family trios. Mutant C1QTNF4 appeared to inhibit some TNF-mediated cellular responses *in vitro*, including NF-κB activation and TNF-induced cell death (10). Very recently this mutation was further reported in a small cohort of Iranian SLE patients, possibly a reflection of the local population structure (11).

Nucleolin is a multidomain shuttling protein with diverse functions, found in the nucleus, cytoplasm, and on the surface of some cells, including cancer cells (12), endothelial cells (13), and monocytic cells (14). Ligands of cell surface nucleolin include Fas (15), lactoferrin (16), growth factors such as midkine (17), lipopolysaccharide (LPS) (18), and viruses such as respiratory syncytial virus (RSV) (19).

Here, we describe the identification of nucleolin as a cell surface receptor of C1QTNF4. We show that the second C1q-like domain in C1QTNF4 is responsible for oligomerization and receptor binding. Monocytes, and to a lesser extent B cells, were found to be target cells of C1QTNF4, and extensive binding of C1QTNF4 to dead cells was observed. C1QTNF4 appears to become internalized upon binding to its receptor. Our data suggest that C1QTNF4 acts within the innate immune system, likely in an anti-inflammatory capacity.

Results

Nucleolin is a cell surface receptor of C1QTNF4

To identify a cell surface receptor of C1QTNF4, we used a recombinant GFP-C1QTNF4 fusion protein produced in

* For correspondence: Timothy J. Vyse, timothy.vyse@kcl.ac.uk.

E. coli as bait. Unfortunately, we were unable to produce unaggregated full-length human C1QTNF4 in mammalian HEK293 cells. Co-immunoprecipitation (co-IP) studies were performed by GFP-Trap with the SK-N-AS neuroblastoma cell line and samples were separated by SDS-PAGE and stained with Coomassie. We identified a band at approximately 100 kDa that was unique to the GFP-C1QTNF4-treated samples (Fig. 1*A*), which was excised and analyzed by liquid chromatography–tandem mass spectrometry (LC-MS/MS) from three independent sample pools. Nucleolin was identified as one of the top hits (Fig. 1*B*) and found to be present in all three samples (Table 1). We confirmed the presence of nucleolin in the co-immunoprecipitate by immunoblotting with an anti-nucleolin antibody and found that nucleolin was considerably more abundant in the GFP-C1QTNF4-treated sample than in the negative control (Fig. 1*C*). The same unique band at around 100 kDa was detected in SDS-PAGE when co-IP was performed from HEK293 cell lysate (Fig. S1*A*) and the presence of nucleolin could again be confirmed by immunoblot (Fig. S1*B*). While nucleolin has a calculated molecular mass of 77 kDa, the protein is known to migrate between 100 and 110 kDa in SDS-PAGE and is prone to autoproteolytic degradation (20, 21). Cell binding of GFP-C1QTNF4 occurred at low to medium affinity in the lower micromolar range (Fig. S1*C*). In order to validate nucleolin as a cell surface receptor of C1QTNF4, we performed siRNA knockdown of nucleolin in HEK293 cells and observed a moderate reduction in GFP-C1QTNF4 binding (Fig. 2, *A* and *B*), which did not entirely mirror the knockdown efficiency observed for nucleolin, both in total cell lysate and on the cell surface (Fig. 2*C*). In contrast to this, knockdown in SK-N-AS cells was not able to reduce GFP-C1QTNF4 binding (Fig. S2, *A*–*C*). We recombinantly produced three soluble multidomain constructs of nucleolin in *E. coli* (Fig. 2*D*) comprising RNA-binding domains 1 to 4 (R1–4) and the glycine/arginine rich (GAR) region, as appropriate, and used these for competition cell-binding assays and *in vitro* co-IP experiments. Both R1234G and R4G were able to compete out

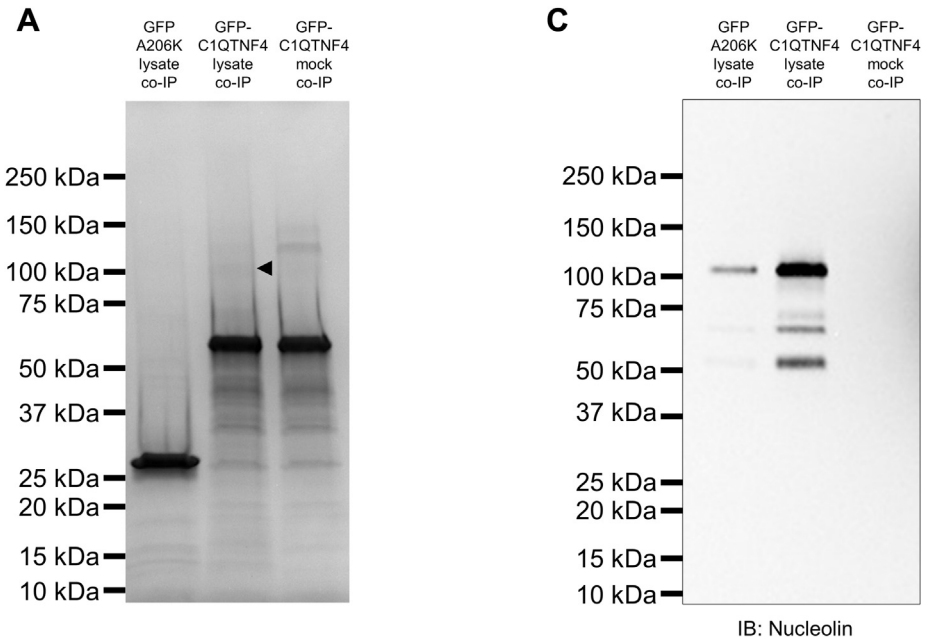

B

>NP_005372.2 nucleolin [*Homo sapiens*]

MVKLAKAGKNQGDPKKMAPPPKEVEEDSEDEEMSEDEEDDSSGEEVVIPQKKGKKAAATSAKKVV
VSPTKK**VAVATPAK**KAAVTPGKKAAATPAKKTVTPAKAVTTPGKKGATPGK**ALVATPGKK**GAAIP
AKGAKNGKNAKKEDSDEEEDDDSEEDEEDDEDEDEDEDEIEPAAMKAAAAAPASEDEDDEDDEDD
EDDDDDEEDDSEEEAMETTPAKGKKAAKVVPVKAKNVAEDEDEEEDDEDEDDDDDEDDEDDDDED
DEEEEEEEEEEPVKEAPGKRKKEMAKQKAAPEAKKQKVEGTEPTTAFNLFVGNLNFNKSAPELK**T**
GISDVFAKNDLAVVDVRIGMTRKFGYVDFESAEDLEK**ALELTGLKVFGNEIK**LEKPKGKDSKKER
DARTLLAKNLPYK**VTQDELK**EVFEDAAEIRLVSKDGKSKGIAYIEFK**TEADAEKTFEEKQGTEID**
GRSISLYYTGEK**GQNQDYR**GGK**NSTWSGESK**TLVLSNLSYSATEETLQEVFEKATFIKVPQNQNG
KSKGYAFIEFASFEDAKEALNSCNKREIEGRAIR**LELQGPR**GSPNARSQPSKTLFVKGLSEDTTE
ETLKESFDGSVRAR**IVTDRETGSSK**GFGFVDFNSEEDAKAAKEAMEDGEIDGNKVTLDWAKPKGE
GGFGGRGGGRGGFGGRGGGRGGRGGFGGRGRGGFGGRGGFRGGRGGGGDHKPQGKKTKFE

Figure 1. Identification of nucleolin as a cell surface receptor of C1QTNF4. *A*, representative image of co-immunoprecipitation reactions of GFP-C1QTNF4 from SK-N-AS cell lysate separated by SDS-PAGE and stained with Coomassie. The band excised for mass spectrometric analysis is indicated by a *black arrowhead*. NCBI reference sequence for C1QTNF4 is NP_114115.2. *B*, amino acid sequence of human nucleolin (NP_005372.2). Peptides detected by mass spectrometry are shown in *bold* and *underlined*. *C*, immunoblot (IB) of co-immunoprecipitation reactions stained with anti-nucleolin.

Table 1
Mass spectrometric results of receptor co-IP

Identified proteins	Accession no.	MW (kDa)	Unique peptide count/Total spectrum count (% coverage)		
			1	2	3
Nucleolin	NUCL_HUMAN	77 kDa	8/8 (9.4%)	8/10 (9.2%)	11/18 (13.1%)
Complement C1q tumor necrosis factor-related protein 4	C1QT4_HUMAN	35 kDa	3/3 (10.9%)	6/8 (21.6%)	7/22 (26.4%)
Gem-associated protein 4	GEMI4_HUMAN	120 kDa		6/7 (6.2%)	11/16 (10.9%)
Probable ATP-dependent RNA helicase DDX20	DDX20_HUMAN	92 kDa		8/10 (12.0%)	7/10 (10.0%)
Trifunctional enzyme subunit alpha, mitochondrial	ECHA_HUMAN	83 kDa			5/5 (6.8%)
Oxysterol-binding protein-related protein 1	OSBL1_HUMAN	108 kDa			5/5 (5.3%)
Fatty acid synthase	FAS_HUMAN	273 kDa			4/4 (2.0%)
Golgi apparatus protein 1	GSLG1_HUMAN	135 kDa			4/4 (4.2%)
Oxysterol-binding protein-related protein 8	OSBL8_HUMAN	101 kDa			4/4 (6.4%)
ATP-binding cassette subfamily F member 1	ABCF1_HUMAN	96 kDa			3/3 (5.3%)
5′-3′ exoribonuclease 2	XRN2_HUMAN	109 kDa			3/3 (4.0%)
Eukaryotic translation initiation factor 3 subunit C	EIF3C_HUMAN	105 kDa			3/3 (4.7%)
Transcription intermediary factor 1-beta	TIF1B_HUMAN	89 kDa			3/3 (7.9%)
General transcription factor 3C polypeptide 3	TF3C3_HUMAN	101 kDa			3/3 (4.5%)

Results shown for proteins identified by LC-MS/MS meeting the following criteria: protein threshold: 99.9%, minimum number of peptides detected: 3, peptide threshold: 95%. Uniprot accession numbers (taxonomy of all identified proteins is *Homo sapiens*), molecular weight (MW, in kDa), unique peptide count, total spectrum count, and protein sequence percent coverage (in brackets) of the identified proteins are provided.

GFP-C1QTNF4 binding to HEK293 cells (Fig. 2*E*), while R123 did not significantly reduce binding of GFP-C1QTNF4. These results provided corroboration that nucleolin is a cell surface receptor of C1QTNF4 and suggested that an interface within RNA-binding domain 4 and the GAR region of nucleolin is involved in the interaction with C1QTNF4. Successful competition of GFP-C1QTNF4 binding with R1234G and R4G was also confirmed in SK-N-AS cells (Fig. S2*D*). To further confirm the specificity of GFP-C1QTNF4's cell binding to nucleolin, we tested competition with the DNA aptamer AS1411 targeting nucleolin (22), and were able to show that GFP-C1QTNF4 binding was completely abrogated (Fig. S2*E*). We performed *in vitro* co-IP between soluble nucleolin construct R1234G and recombinant full-length C1QTNF4 and were able to show direct interaction between nucleolin and C1QTNF4 (Fig. 2*F*).

Domain 2 of C1QTNF4 mediates oligomerization

C1QTNF4 is unique within the C1QTNF and wider C1q-like domain-containing family by being made up of two C1q-like domains in tandem. To investigate the contributions of the two domains, we produced single-domain constructs of C1QTNF4 in *E. coli* (Fig. S3*A*). Domain 2 on its own tended to precipitate, even more so than full-length C1QTNF4, and thus GFP A206K-tagged constructs (Fig. S3*B*) were compared. While GFP can form dimers at high concentrations (23), GFP A206K has been engineered as a monomer, with a very high micromolar dissociation constant (24) and therefore does not contribute to oligomerization at the concentrations used here. To determine the oligomerization state of C1QTNF4 constructs, we performed size-exclusion chromatography (SEC) with multiangle laser light scattering (SEC-MALLS) experiments. We observed that domain 1 of C1QTNF4 was mainly present in monomeric form (Fig. 3*A*), while full-length C1QTNF4 predominantly formed monomers and trimers, but was also present as likely hexamers and higher-molecular-weight species. Both GFP-tagged domain 1 and GFP-C1QTNF4 showed similar behavior to their untagged counterparts, although GFP-C1QTNF4 predominantly formed trimers and higher-molecular-weight species (Fig. S4*A*). GFP-tagged domain 2 formed large oligomers, based on these and further results possibly nonamers with distorting higher-molecular-weight species present. Nevertheless, it is possible that domain 2 forms multiple main oligomeric states. To test whether domains 1 and 2 of C1QTNF4 interact, we performed SEC of a 1:1 molar ratio of the two GFP-domain fusion constructs at 10 μM. However, we did not detect any interaction at medium to high affinity, as would be discernible by SEC (Fig. 3*B*). This suggests that oligomerization of C1QTNF4 is driven by domain 2, as domain 1 was found in monomeric form and there was no high affinity interaction between the domains.

Domain 2 of C1QTNF4 is responsible for receptor binding

To investigate which of the domains is involved in binding to C1QTNF4's receptor, we performed cell-binding experiments with the different GFP fusion constructs (Fig. 3*C*). Neither the GFP A206K control nor the GFP-C1QTNF4 domain 1 bound to cells. However, GFP-C1QTNF4 domain 2 bound to cells but it was not able to reproduce full-length GFP-C1QTNF4 binding, which could be due to differences in oligomerization state. *In vitro* co-IP experiments between GFP fusion constructs of C1QTNF4 and soluble nucleolin constructs confirmed that domain 2 and R4G appeared to be responsible for the interaction between C1QTNF4 and nucleolin, respectively (Fig. 3*D*). C1QTNF family members are known to form trimers as a basic structural unit (25) and oligomer-dependent functions of adiponectin have been reported (26, 27). While C1QTNF4 was found in different oligomeric forms, we were unable to identify one single active oligomeric species involved in receptor binding. Different oligomeric states of GFP-C1QTNF4, with what are likely trimeric, hexameric, and higher-molecular-weight species, bound to the receptor similarly well (Fig. S4*B*). The binding of monomeric GFP-C1QTNF4 was lower than oligomeric forms, but this is likely due to a lack of avidity of the monomeric form as well as a reduced overall fluorescence of the monomer.

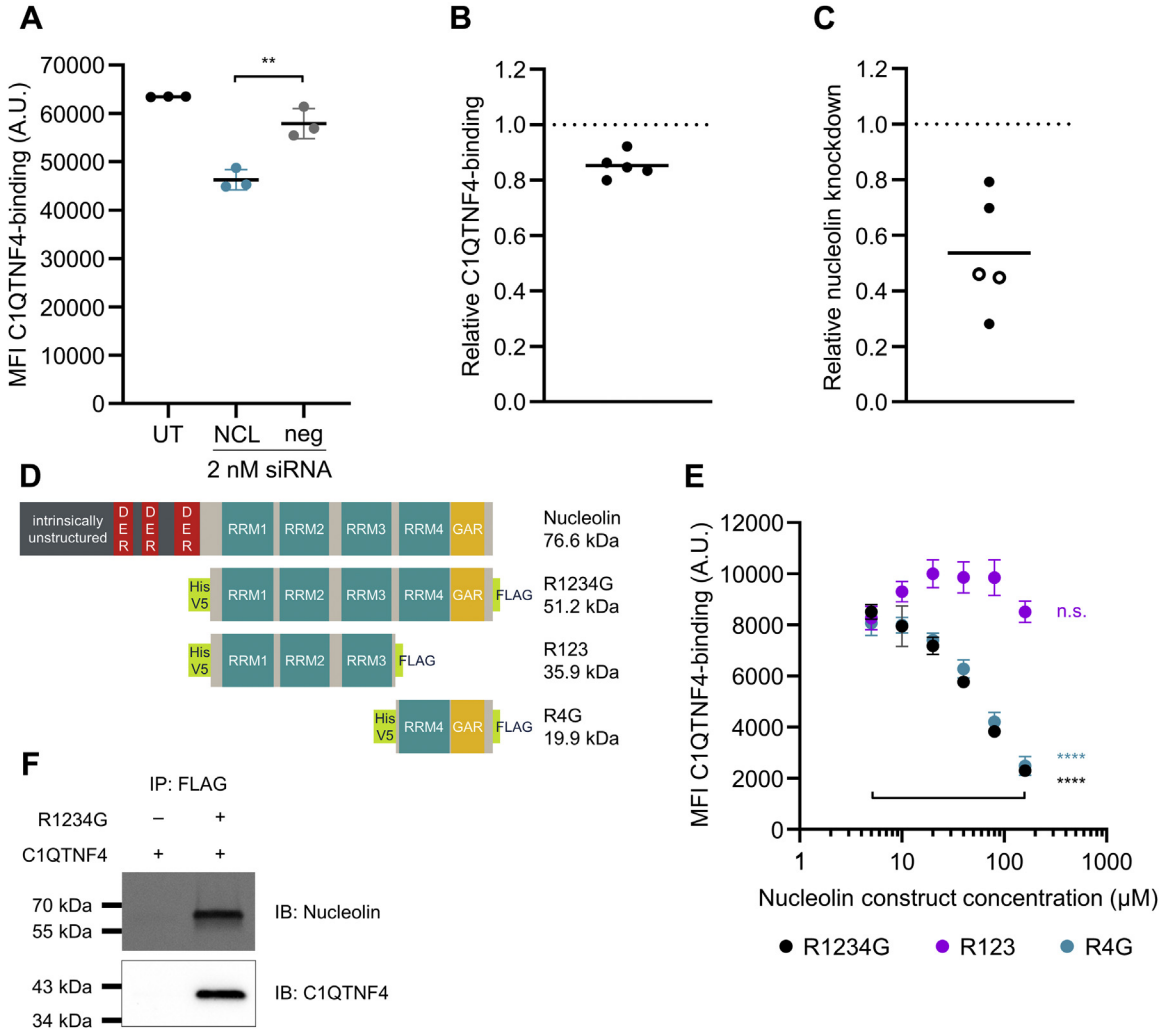

Figure 2. Validation of nucleolin as a cell surface receptor of C1QTNF4. *A*, GFP-C1QTNF4 binding to HEK293 at 5 μM was quantified by flow cytometry and MFI was plotted according to siRNA treatment. UT, untreated; NCL, nucleolin siRNA at 2 nM; neg: negative siRNA at 2 nM, n = 3 technical replicates. The mean is represented as a horizontal bar, with the error bars above and below denoting the standard deviation. $^{**}p < 0.01$, by ordinary one-way ANOVA with Tukey's multiple comparisons test. *B*, relative GFP-C1QTNF4-binding as a ratio of the mean of nucleolin and negative siRNA MFI for five binding experiments performed in HEK293, each n = 3 technical replicates. *C*, relative nucleolin knockdown as a ratio of nucleolin and negative siRNA. Knockdown was assessed by immunoblot (*filled circles*, ratio calculated from nucleolin/actin) or flow cytometric cell surface staining of nucleolin (*empty circles*) and performed alongside all five binding experiments carried out in HEK293, each n = 1. *D*, schematic representation of full-length nucleolin and the three recombinantly produced nucleolin constructs R1234G (aa 285–710), R123 (aa 285–561), and R4G (aa 566–710) in pET151. *E*, competition of GFP-C1QTNF4-binding with nucleolin constructs R1234G (*black circles*), R123 (*purple circles*), and R4G (*turquoise circles*) using HEK293 cells. Mean shown with error bars denoting the standard deviation, n = 3 technical replicates. $^{****}p < 0.0001$, n.s., nonsignificant, by unpaired *t*-test comparing lowest with highest concentration of each nucleolin construct. *F*, *in vitro* co-immunoprecipitation of FLAG-tagged R1234G by anti-FLAG affinity resin. Immunoblot stained with anti-nucleolin and anti-C1QTNF4. A.U., arbitrary units; IB, immunoblot; MFI, median fluorescence intensity.

We investigated the impact of the H198Q mutation discovered in SLE, which is located in the second C1q-like domain of C1QTNF4. We did not observe any differences between the binding of wild-type and mutant H198Q GFP-C1QTNF4 in the cell-binding assays we performed (Fig. S5*A*), within the limitations of the sensitivity of the binding assays conducted. Further, we detected no obvious impact of the H198Q mutation on the oligomerization capacity of GFP-C1QTNF4 (Fig. S5*B*), with only small differences in oligomeric proportions observed, possibly due to batch effects, which confirms what has previously been reported for C1QTNF4 expressed in mammalian cells (10).

Monocytes and B cells are target cells of C1QTNF4

To investigate the cellular target cells of C1QTNF4 and to assess the expression of cell surface nucleolin in immune cell subsets, we performed flow cytometric analysis of peripheral blood mononuclear cells (PBMCs) from a healthy female. Monocytes bound high levels of GFP-tagged C1QTNF4, while a subset of B cells and a very small percentage of T cells (approximately 1%) were positive for C1QTNF4 binding (Fig. 4*A*). This mirrored the cell surface expression pattern observed for nucleolin, with monocytes uniformly expressing nucleolin on their cell surface, a subset of B cells (here approximately 29%) and a very small subset of T cells (1–2%)

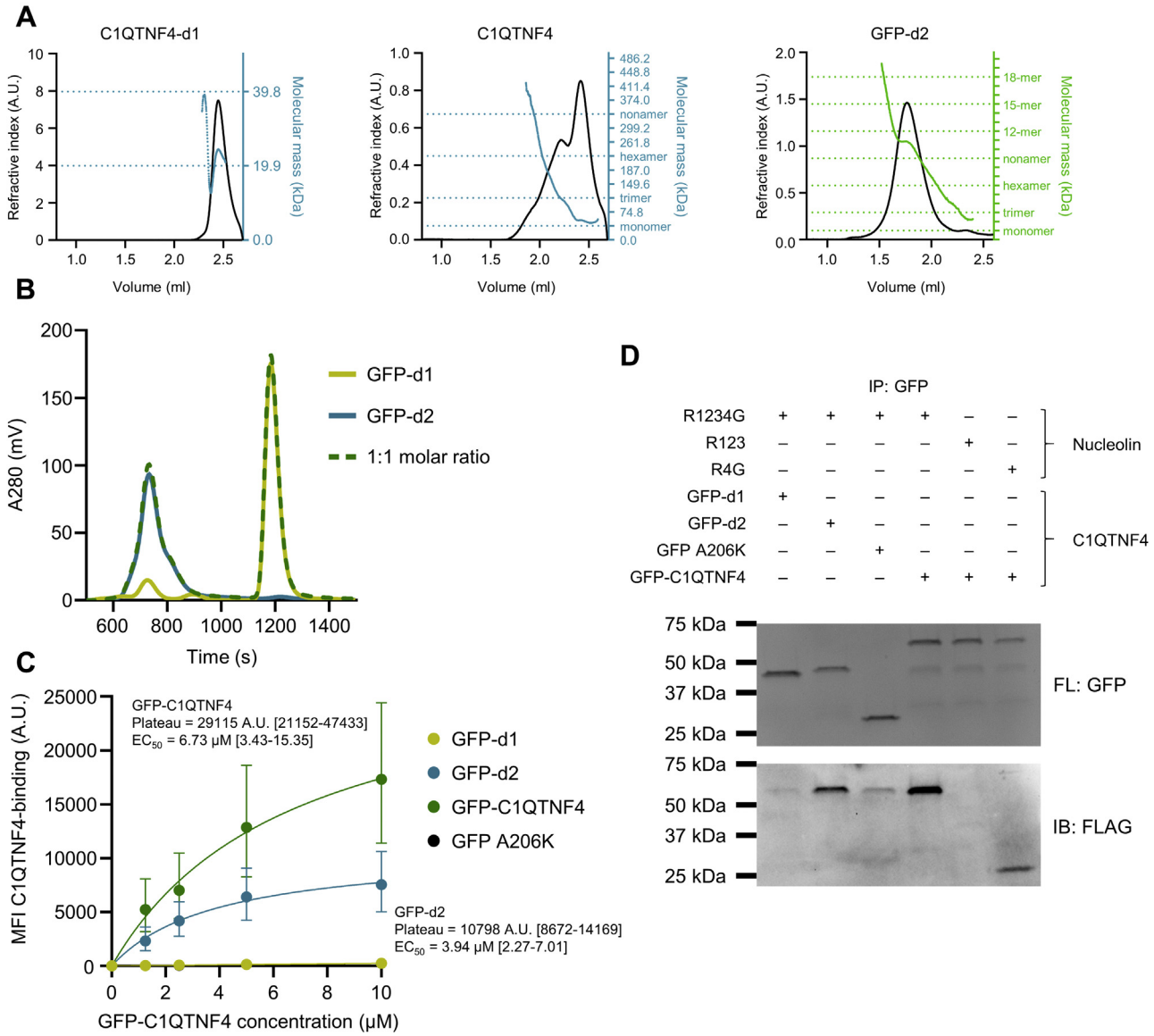

Figure 3. Oligomerization and domain binding of C1QTNF4. *A*, SEC-MALLS chromatograms of C1QTNF4 domain 1 (C1QTNF4-d1), full-length C1QTNF4, and GFP-C1QTNF4 domain 2 (GFP-d2). The Y-axes indicate refractive index (shown in *black*) and molecular mass (in kDa shown in *turquoise* or *green*), with ticks in monomeric molecular mass. *B*, chromatogram showing 10 μM GFP-C1QTNF4 domain 1 (GFP-d1) and GFP-C1QTNF4 domain 2 (GFP-d2) individually or at 1:1 molar ratio to assess interaction of the two domains. *C*, MFI values of GFP-C1QTNF4 constructs binding to HEK293 are plotted, with error bars denoting the interquartile range. Top plateau and EC_{50} values were fit, with 95% confidence intervals shown in *square brackets*. Data points for GFP A206K are obscured by near-identical data points for GFP-d1. *D*, immunoprecipitation of GFP fusion constructs of C1QTNF4 by GFP-Trap Agarose. Immunoblot showing autofluorescence of GFP constructs and stained with anti-FLAG to detect nucleolin constructs. A.U., arbitrary units; A280, absorbance at 280 nm; FL, autofluorescence; IB, immunoblot; MFI, median fluorescence intensity.

staining positive for cell surface nucleolin (Fig. 4*B* and Fig. S6*A* for gating strategy).

C1QTNF4 extensively binds to dead cells

Interestingly, we observed binding of C1QTNF4 to dead cells. Failure to clear apoptotic cells is one of the pathways that can underlie SLE pathogenesis (28), and C1q itself is known to directly bind to apoptotic cells *via* its globular head domain and to be involved in their clearance (29–31). Furthermore, nucleolin on the surface of macrophages can bind to early apoptotic Jurkat T cells through carbohydrate chains on capped CD43 (14). To investigate whether C1QTNF4 is involved in apoptotic cell clearance, we tested binding of GFP-C1QTNF4 to staurosporine-induced apoptotic Jurkat T cells. Little binding of GFP-C1QTNF4 was observed to live or early apoptotic Jurkat T cells (Fig 5*A* and Fig. S6*B* for gating strategy), and this was mirrored with little cell surface staining seen for nucleolin on these subsets (Fig. 5*B*). In contrast, dead (late apoptotic) cells strongly and uniformly bound C1QTNF4. While dead cells are known to be "sticky" and thus routinely excluded from flow cytometric analysis, we observed binding of GFP-C1QTNF4 considerably above what was observed for GFP alone, suggesting a functional role. Nucleolin staining on these cells was also extensive, suggesting that nucleolin is

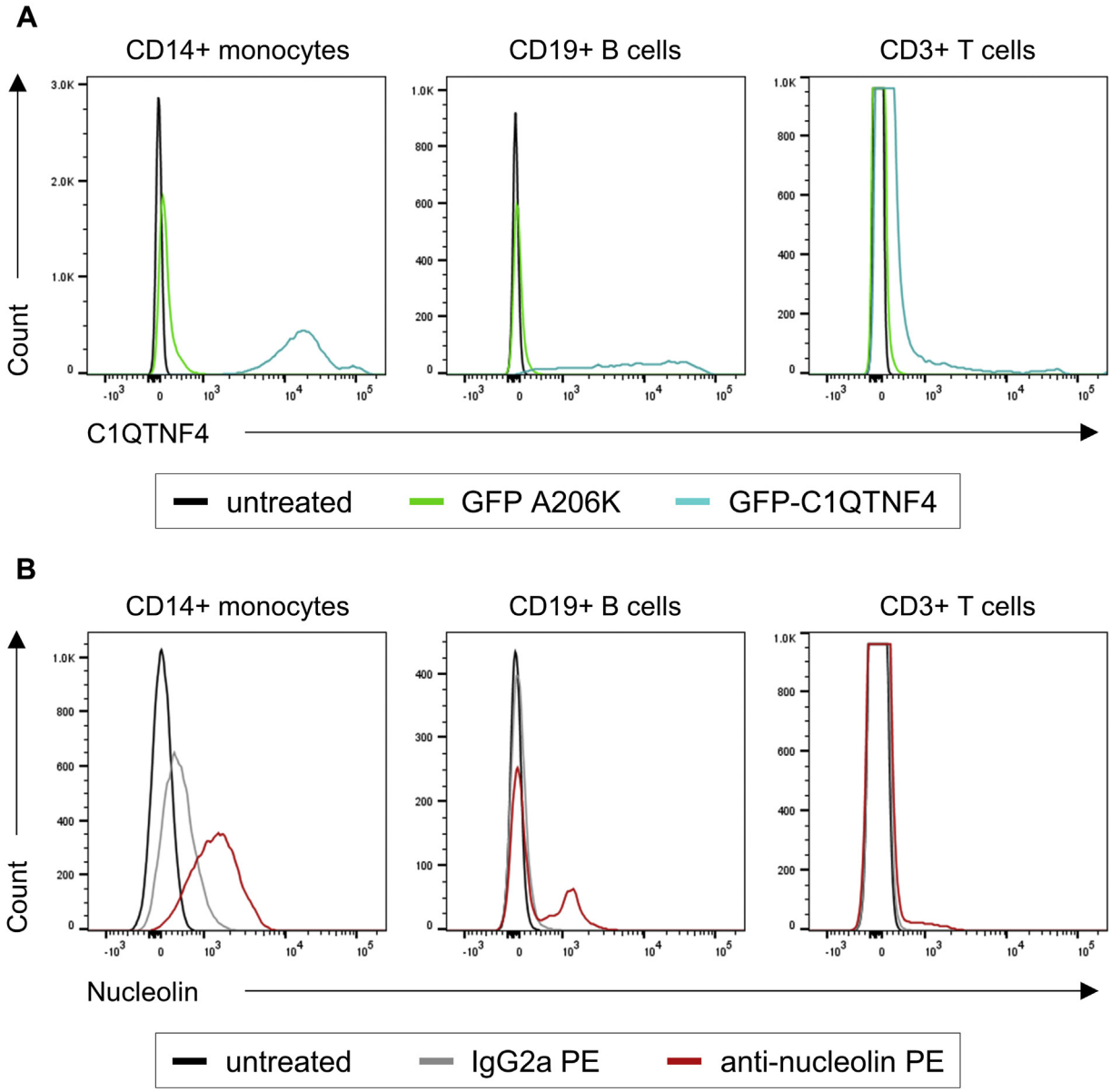

Figure 4. GFP-C1QTNF4 binding and nucleolin cell surface expression on PBMC subsets. *A*, GFP-C1QTNF4 binding to CD14+ monocytes, CD19+ B cells, and CD3+ T cells. Untreated (*black*), 5 μm GFP A206K control (*green*), and 5 μM GFP-C1QTNF4 (*turquoise*). *B*, nucleolin surface staining in CD14+ monocytes, CD19+ B cells, and CD3+ T cells. Untreated (*black*), isotype control (*gray*), anti-nucleolin (*red*).

accessible on dead cells and possibly an immunologically relevant target of C1QTNF4.

Internalization of C1QTNF4

Ligands of nucleolin have been reported to become actively internalized upon receptor binding, including lactoferrin (16). We assessed internalization of GFP-C1QTNF4 in CD14+ monocytes by imaging flow cytometry, comparing incubation on ice with incubation at 37 °C. GFP-C1QTNF4 localized to the membrane of monocytes after incubation on ice (Fig. 6*A*), while pronounced intracellular GFP-C1QTNF4 localization was observed after incubation at 37 °C (Fig. 6*B*), with a higher internalization score calculated (Fig. 6*C*). We performed similar experiments in HEK293 cells by microscopy and again found that GFP-C1QTNF4 localized to the cell membrane after incubation on ice (Fig. S7*A*), while highly fluorescent punctae were observed after incubation at 37 °C (Fig. S7*B*). No binding or internalization was observed for control GFP A206K (Fig. S7, *C* and *D*). These results suggest that C1QTNF4 becomes actively internalized as a result of receptor binding.

Relationship to inflammation

As we were able to show that C1QTNF4 interacts with the C-terminal region of nucleolin, which has been implicated in ligand binding of many other molecules, including lactoferrin (16), midkine (32), and Fas (15), we wanted to explore whether lactoferrin and C1QTNF4 compete for binding. We found that lactoferrin was able to completely abrogate binding of GFP-C1QTNF4 to *ex vivo* monocytes (Fig. 6*D*) and HEK293 cells (Fig. S8*A*), suggesting that the two ligands compete for the

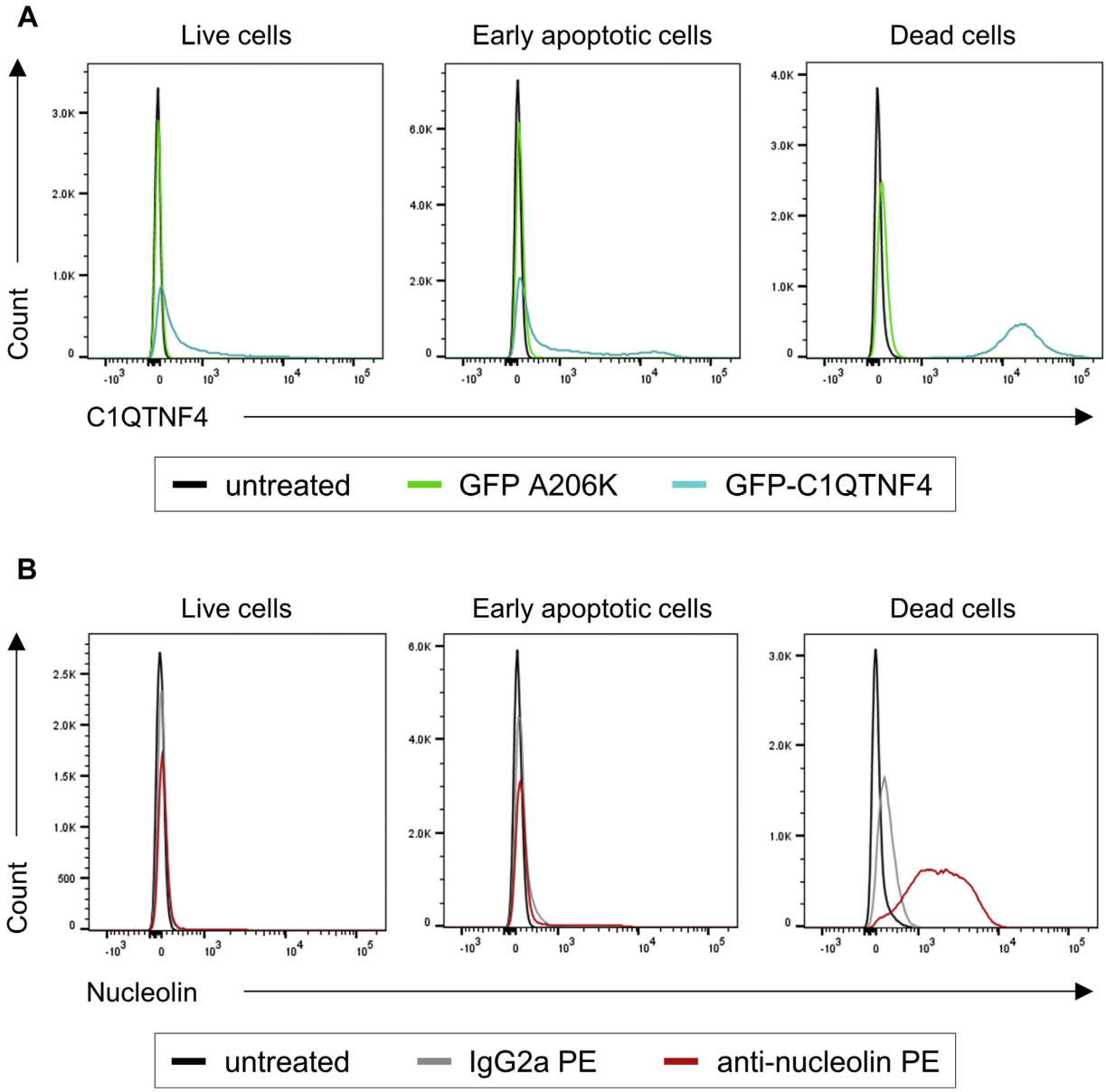

Figure 5. Exploring a link to apoptotic cell clearance. *A*, GFP-C1QTNF4 binding to live, early apoptotic, and dead cells. Untreated (*black*), 5 μm GFP A206K control (*green*), and 5 μM GFP-C1QTNF4 (*turquoise*). *B*, nucleolin surface staining in live, early apoptotic, and dead cells. Untreated (*black*), isotype control (*gray*), anti-nucleolin (*red*).

same binding site on nucleolin. LPS, a reported ligand of nucleolin (18), was not able to compete with GFP-C1QTNF4 for binding (Fig. S8*B*), suggesting either a differential binding interface or competition by C1QTNF4.

Discussion

As a crucial aspect to understanding C1QTNF4's functions, a cell surface receptor of C1QTNF4 had hitherto not been discovered. In this study, we identify nucleolin as a cell surface receptor of C1QTNF4, which can be found on monocytes and some B cells, among other cells. Nucleolin lacks a transmembrane domain, and it is currently unclear how it associates with the plasma membrane. Nucleolin may thus serve as a docking molecule for C1QTNF4, acting in a context-dependent manner through coreceptors. This might account for the differences in GFP-C1QTNF4 binding observed in different cell types upon nucleolin knockdown, as competition with soluble nucleolin effectively reduced cell binding in both HEK293 and SK-N-AS cells. The interaction between C1QTNF4 and nucleolin seems to be mediated by the C terminus of nucleolin and appears to be of low to medium affinity; this is in accordance with what has been described for other ligands of nucleolin, including lactoferrin (16), midkine (32), and pleiotrophin (33). In contrast to some of these other nucleolin ligands, which have additional high-affinity receptors, GFP-C1QTNF4 binding was much reduced by soluble nucleolin and completely abrogated by both lactoferrin and the DNA aptamer AS1411. It is currently unclear whether and how

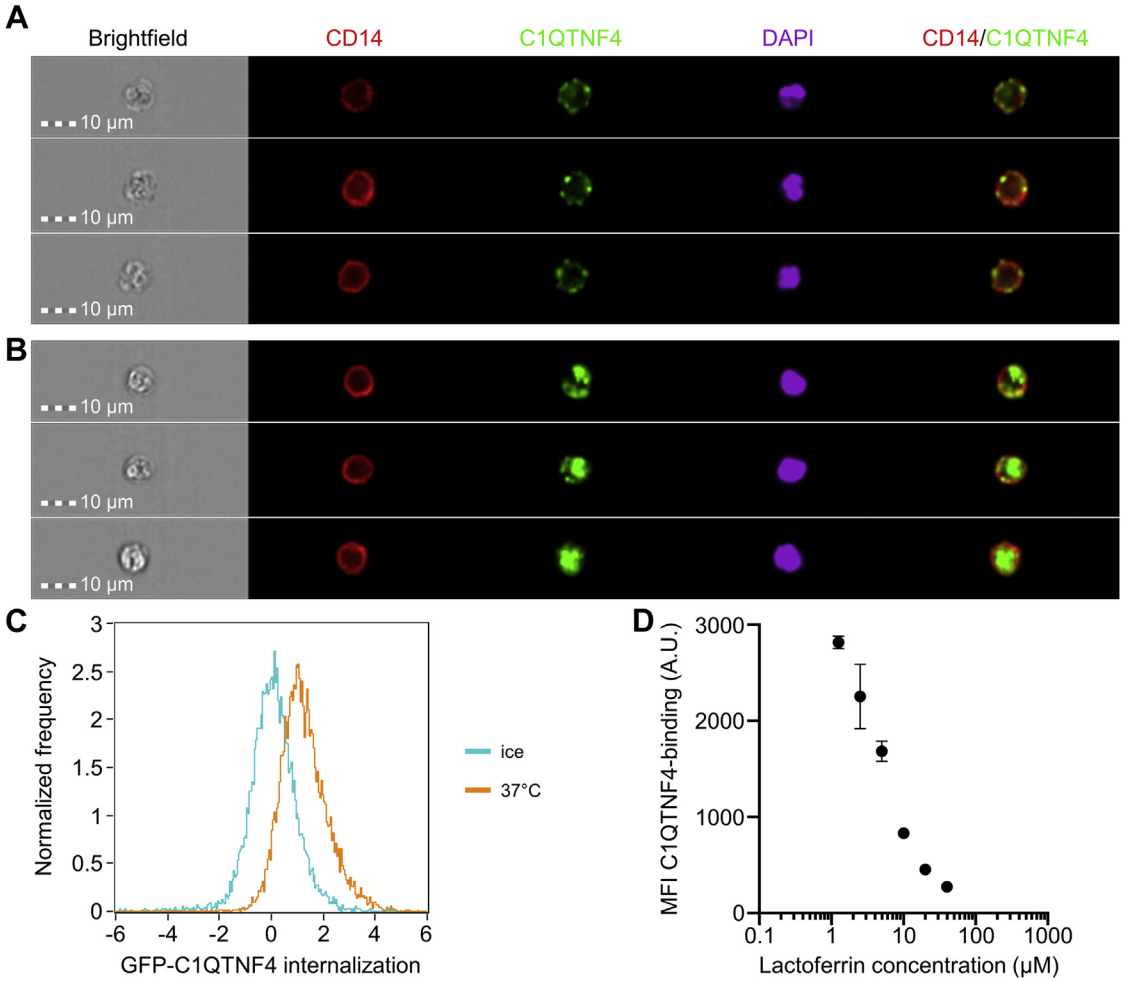

Figure 6. Internalization of GFP-C1QTNF4 in monocytes. *A* and *B*, CD14+ monocytes (*red*) were imaged after incubation with 1.25 µM GFP-C1QTNF4 (*green*), (*A*) on ice or (*B*) at 37 °C. Nuclei were stained with DAPI (*purple*). The merged image shows the CD14 and GFP-C1QTNF4 staining used to assess internalization. Three representative images are shown for each condition. Scale bar represents 10 µm. *C*, GFP-C1QTNF4 internalization score as calculated by the IDEAS software, n = ~10,000 CD14+ monocytes. A higher score represents more internalization. *D*, competition of GFP-C1QTNF4-binding with lactoferrin in *ex vivo* monocytes. The mean is shown with error bars denoting the standard deviation, n = 3 technical replicates. A.U., arbitrary units; MFI, median fluorescence intensity.

C1QTNF4 impacts on functions of other nucleolin ligands, and vice versa. Nucleolin has been identified as part of a multiprotein signaling complex containing annexin A2, calreticulin, and TLR4 on the surface of endothelial cells (34), as well as in complex with heat shock proteins (including HSPA1A), TLR2, and TLR4 on the cell surface of THP-1 cells (35). Further, TLR4 may act as a coreceptor of nucleolin in cellular entry of RSV (36, 37). Both nucleolin (18) and TLR4 in conjunction with MD-2 and CD14 (38) have been reported or are known to bind LPS, and engagement of TLR4 can stimulate IL-6 and TNF-α production (39, 40). Interestingly, lactoferrin has been shown to bind to nucleolin (16) and reported to act through TLR4, both independently and in an LPS-dependent manner (41). While there is currently no evidence that C1QTNF4 signals directly through TLR4, this is an avenue that warrants further exploration, as TLR4 could be a potential candidate for mediating C1QTNF4's functions into the cell. There are conflicting reports concerning C1QTNF4's functions. Overexpression of C1QTNF4 in HEK293T cells upregulates NF-κB activity, and C1QTNF4 has been reported to increase the expression of proinflammatory molecules such as IL-6 and TNF-α in HepG2 cells (3), while C1QTNF4 has been shown to reduce LPS-mediated IL-6 and TNF-α production in murine macrophages (4). Furthermore, C1QTNF4 appears to compete with LPS for binding to its receptors on macrophages, and *C1qtnf4* knockout mice are more susceptible to LPS-induced systemic inflammation (42). Based on the results presented here, C1QTNF4 may act in a coreceptor-, context-, or oligomer-dependent manner after binding to nucleolin, likely facilitating anti-inflammatory actions within the innate immune system. While receptors for some C1QTNF family members have been identified, no other C1QTNF molecule has been described to bind to nucleolin. However, C1QTNF3 and C1QTNF9 have been reported to bind to TLR4/MD-2, acting as LPS antagonists (43, 44). Both nucleolin (12) and TLR4 (45) can become actively internalized upon ligand binding and here we could show that C1QTNF4 becomes internalized as part of an active process. Furthermore, it has very recently been suggested that C1QTNF4 affects TLR4 endocytosis (42). C1QTNF4 might therefore perform direct signaling functions and indirectly act

by blocking or removing the nucleolin receptor complex for proinflammatory ligands. C1QTNF4 might further have antiviral properties by preventing the binding of viruses such as RSV to nucleolin for cellular entry. While C1QTNF4 does not appear to be directly involved in early apoptotic cell clearance, it may modulate nucleolin's function on the surface of macrophages where it has been reported to bind to early apoptotic cells through carbohydrate chains on capped CD43 (14). It will be of future interest to explore whether C1QTNF4 is involved in the clearance of dead cells.

Previously, the roles of the individual domains of C1QTNF4 had not been examined and we were able to show that the second C1q-like domain mediated C1QTNF4's oligomerization and receptor-binding functions, while the contribution of domain 1 to function remained unclear. Byerly *et al.* (6) had previously assessed oligomerization of murine full-length C1QTNF4 produced in HEK293T cells and showed that C1QTNF4 was present in multiple species, likely trimers, hexamers, and higher-molecular-weight species. While we were not able to produce unaggregated human C1QTNF4 in mammalian HEK293 cells, our results for C1QTNF4 produced in bacterial cells were similar; however, monomeric C1QTNF4 could also be detected. In order to assess the impact of a H198Q mutation within the second C1q-like domain, initially discovered in a single SLE patient (10) and further identified in an Iranian SLE cohort (11), we compared cell binding between wild-type and mutant C1QTNF4. Within the limitations of the experiments conducted, we were not able to detect obvious differences between wild-type and mutant GFP-C1QTNF4 H198Q. While this mutation was never proved to be causal, it is likely that downstream events following receptor binding are instead impacted. Other C1QTNF family members have been implicated in autoimmunity, including C1QTNF1 (46), C1QTNF3 (47), and C1QTNF6 (48–51), which also has a suggestive association with SLE (52). Interestingly, both C1QTNF3 and C1QTNF6 appear to be protective toward autoimmunity. Taken together, this suggests that loss of function of C1QTNF4 may predispose to autoimmunity.

While there is some uncertainty as to the cellular source of human C1QTNF4, there is a consensus that *C1QTNF4* is expressed in the brain (6), with GTEx RNA sequencing data (53) and BioGPS microarray data (54–56) corroborating this, and *C1QTNF4* may be expressed in adipose tissue (6). Further, *C1QTNF4* appears to be expressed in hematopoietic stem and progenitor cells (54, 57, 58) and coexpressed with CD34 in COEXPRESdb Hsa microarray data (59). Interestingly, nucleolin is enriched in CD34+ hematopoietic stem and progenitor cells (60, 61), and overexpression of nucleolin in these cells leads to transcriptional downregulation of genes associated with immunity and inflammation (62). While C1QTNF4 is highly conserved among vertebrates, there appears to be a marked difference between human and mouse tissue expression of C1QTNF4, with mouse *C1QTNF4* abundant in the testis, kidney, and brain (6), but no expression reported in hematopoietic progenitor cells in BioGPS microarray data (54). Knockout of *C1qtnf4* in a mouse model does not affect immune cell composition, suggesting that C1QTNF4 is not required for normal development of the murine immune system. Interestingly, C1QTNF4 appears to have sex-dependent physiological actions relating to food intake and metabolism (8). It remains unclear whether the mouse is an appropriate model organism to study C1QTNF4's immune-related functions in humans. Interestingly, GTEx RNA sequencing data suggest that in humans, *C1QTNF4* is expressed at higher levels in males than females (53). Taken together, sexually dimorphic actions of C1QTNF4 may be of functional relevance for a disease such as SLE that has a striking female-biased sex imbalance. Noteworthy, an intracellular C1QTNF4 orthologue has been described in red-lip mullet fish, which showed highest expression in peripheral blood cells and was upregulated in response to bacteria and pathogen-associated molecular patterns, including LPS and may thus be part of the innate immune response (63). Our data further support C1QTNF4 as an actor within the innate immune system in humans, likely in an anti-inflammatory capacity.

Despite the recent emergence of putative roles relating to cancer and metabolism, C1QTNF4's physiological functions have remained poorly studied. This study provides a further step to understanding C1QTNF4's function in the healthy immune system and how dysfunction may contribute to the development of SLE.

Experimental procedures

Protein expression and purification

Amino acids 17 to 329 (full-length), 17 to 167 (domain 1), and 168 to 329 (domain 2) of human C1QTNF4 were cloned into pET151 (Thermo Fisher Scientific). They were further cloned as GFP-C1QTNF4 fusion constructs into pET151 containing an N-terminal eGFP A206K domain followed by a short serine-glycine linker using polymerase incomplete primer extension cloning (64), named GFP-C1QTNF4 (aa 17–329), GFP-d1 (aa 17–167), and GFP-d2 (aa 168–329). eGFP A206K was also separately expressed in pET151. Site-directed mutagenesis for H198Q was performed using a QuikChange Lightning Kit (Agilent) according to the manufacturer's instructions with 5'-GGGCCGCGGCAGCAACCACTCGC-3' (Integrated DNA Technologies). Three constructs of human nucleolin, codon-optimized for *E. coli* (GeneArt), were cloned into pET151 with an additional C-terminal GSSDYKDDDDK tag: R1234G (aa 285–710), R123 (aa 285–561), and R4G (aa 566–710). Constructs and mutations were verified by Sanger sequencing (Eurofins Genomics). Proteins were expressed in BL21 Star DE3 *E. coli* (Thermo Fisher Scientific) grown in ZYP-5052 autoinduction medium (65) at 18 °C. They were purified *via* their hexahistidine tags with HisTrap FF Crude columns (Cytiva) and where appropriate further purified by SEC using a Superdex 200 Increase 10/300 GL column (Cytiva).

Cell culture and siRNA transfection

The HEK293 cell line was cultured in DMEM containing 2 mM L-glutamine supplemented with 10% heat-inactivated

fetal bovine serum (FBS), 100 U/ml penicillin, and 100 μg/ml streptomycin. The neuroblastoma SK-N-AS cell line was cultured in RPMI-1640 medium containing 2 mM L-glutamine, 10% heat-inactivated FBS, 100 U/ml penicillin, 100 μg/ml streptomycin (all Thermo Fisher Scientific), and 1 mM sodium pyruvate (Sigma-Aldrich). The cells were grown in a humidified incubator at 37 °C with 5% CO_2 and routinely passaged with trypsin/EDTA (Sigma-Aldrich). For binding experiments, cells were instead harvested with 0.526 mM EDTA in Dulbecco's PBS.

Knockdown of nucleolin was performed using Silencer Select s9312 against nucleolin (sense 5'-GGAUAGUUACUGACCGGGAtt-3') and Silencer Select Negative Control No. 1 siRNA (both Thermo Fisher Scientific). Cells were seeded 24 h before transfection with INTERFERin (Polyplus Transfection) according to the manufacturer's instructions. Cells were harvested 72 h post transfection.

Receptor identification by co-immunoprecipitation

Per reaction, 5 to 10 × 10^7 SK-N-AS cells were used for receptor identification, with exogenously added GFP-C1QTNF4 or control GFP A206K used as bait. Cells were lysed in 25 mM Tris-HCl pH 7.4, 150 mM NaCl, 1% Triton X-100, 5% glycerol, supplemented with 1X protease inhibitor (Roche) at 4 °C, and co-IP from cleared lysate performed by incubation with 10 μl washed GFP-Trap Agarose (ChromoTek) for 2 h at 4 °C. Beads were washed three times in 25 mM Tris-HCl pH 7.4, 150 mM NaCl, 1% Triton X-100, 5% glycerol, and bound proteins were eluted by boiling in reducing 2X Laemmli sample buffer. Samples were separated on a 4 to 15% Mini-PROTEAN TGX gel (Bio-Rad), stained with InstantBlue Coomassie stain (Expedeon), relevant bands excised and analyzed by LC-MS/MS.

LC-MS/MS

Enzymatic digestion

In-gel reduction, alkylation, and digestion with trypsin were performed on selected gel bands prior to subsequent analysis by mass spectrometry. Cysteine residues were reduced with dithiothreitol and derivatized by treatment with iodoacetamide to form stable carbamidomethyl derivatives. Trypsin digestion was carried out overnight at room temperature after initial incubation at 37 °C for 2 h.

LC-MS/MS

Peptides were extracted from the gel pieces by a series of acetonitrile and aqueous washes. The extract was pooled with the initial supernatant and lyophilized. The sample was then resuspended in 40 μl of resuspension buffer (2% acetonitrile in 0.05% formic acid) and analyzed by LC-MS/MS (10 μl). Chromatographic separation was performed using a U3000 UHPLC NanoLC system (Thermo Fisher Scientific). Peptides were resolved by reversed-phase chromatography on a 75 μm C18 Pepmap column (50 cm length) using a three-step linear gradient of 80% acetonitrile in 0.1% formic acid. The gradient was delivered to elute the peptides at a flow rate of 250 nl/min over 60 min starting at 5% B (0–5 min) and increasing solvent to 40% B (5–40 min) prior to a wash step at 99% B (40–45 min) followed by an equilibration step at 5% B (45–60 min). The eluate was ionized by electrospray ionization using an Orbitrap Fusion Lumos (Thermo Fisher Scientific) operating under Xcalibur v4.1.5. The instrument was first programmed to acquire using an Orbitrap-Ion Trap method by defining a 3 s cycle time between a full MS scan and MS/MS fragmentation. Orbitrap spectra (FTMS1) were collected at a resolution of 120,000 over a scan range of m/z 375 to 1500 with an automatic gain control setting of 4.0e5 with a maximum injection time of 35 ms. Monoisotopic precursor ions were filtered using charge state (+2 to +7) with an intensity threshold set between 5.0e3 and 1.0e20 and a dynamic exclusion window of 35 s ±10 ppm. MS2 precursor ions were isolated in the quadrupole set to a mass width filter of 1.6 m/z. Ion trap fragmentation spectra (ITMS2) were collected with an automatic gain control target setting of 1.0e4 with a maximum injection time of 35 ms with CID collision energy set at 35%.

Data processing

Raw mass spectrometry data were processed using Proteome Discoverer v2.2 and the data searched against the Human Taxonomy Uniprot database (release 2018_06, 20,293 entries and release 2019_08, 20,368 entries) using the Mascot v2.6.0 (Matrix Science) and Sequest (66) search algorithms. Trypsin specifically cuts at lysine and arginine residues, and a maximum of two missed tryptic cleavages were permitted. Carbamidomethyl on cysteine residues was considered as a fixed modification, and oxidation on methionine residues was considered as a variable modification. Searching was performed with a fragment ion mass tolerance of 0.60 Da and a parent ion tolerance of 10.0 ppm. Protein identifications in Scaffold v4.8.4 were reported at a threshold of 99.0%, with a minimum of three peptides assigned per protein, at a peptide threshold of 95%. The Prophet false discovery rate was estimated at 0.8% for peptides.

In vitro *co-immunoprecipitation*

In vitro co-IP was performed for purified C1QTNF4 and purified nucleolin constructs to assess direct interaction. For IP with FLAG affinity resin, 50 nM R1234G was mixed with 200 nM C1QTNF4 and incubated overnight at 4 °C on an end-to-end rotator. For IP by GFP-Trap Agarose, 50 nM C1QTNF4 constructs were mixed with 200 nM nucleolin constructs in 25 mM Tris-HCl pH 7.4, 150 mM NaCl, 1% Triton X-100, 5% glycerol and incubated for 2 h at 4 °C on an end-to-end rotator. In total, 10 μl washed anti-FLAG affinity resin (Sigma-Aldrich) or 5 μl washed GFP-Trap Agarose was added and incubated for a further 2 h at 4 °C. The beads were collected and washed three times in 25 mM Tris-HCl pH 7.4, 150 mM NaCl, 1% Triton X-100, 5% glycerol. Bound protein was eluted by boiling in reducing 2X Laemmli sample buffer at 95 °C for 10 min. Samples were analyzed by immunoblot.

Immunoblot

HEK293 and SK-N-AS cell lysates were prepared in 25 mM Tris-HCl pH 7.4, 150 mM NaCl, 1% Triton X-100, 5% glycerol,

supplemented with 1X protease inhibitor (Roche). Cells were incubated in lysis buffer on ice, then scraped and centrifuged for 10 min at 20,000*g* and 4 °C to remove cellular debris. Samples were separated on a 4 to 15% Mini-PROTEAN TGX gel (Bio-Rad), the proteins transferred onto a nitrocellulose membrane (Cytiva) and blocked in 5% milk in PBS. Primary antibody detection was performed in 1% milk in 0.05% Tween in PBS at 4 °C and secondary detection at room temperature. Blots were developed using Luminata Crescendo Western HRP substrate (Merck Millipore) and imaged using an iBright FL1000 Imaging System (Thermo Fisher Scientific). Primary antibodies used were rabbit anti-C1QTNF4 (Abcam, ab36871) at 1:1000, mouse anti-nucleolin H-6 (Santa Cruz Biotechnology, sc-55486) at 1:1000, mouse anti-β-actin (Santa Cruz Biotechnology, sc-47778) at 1:4000, and mouse anti-FLAG M2 (Sigma-Aldrich, F1804) at 1:1000. Secondary antibodies used were highly cross-adsorbed goat anti-rabbit IgG HRP at 1:10,000 (Thermo Fisher Scientific, A16110) and goat anti-mouse IgG HRP (Abcam, ab97023) at 1:10,000. For fluorescent detection, membranes were incubated in primary anti-nucleolin H-6 PE (Santa Cruz Biotechnology, sc-55486 PE) at 1:1000 and imaged directly after washing.

PBMC and monocyte isolation

PBMCs were separated from whole blood using Histopaque-1077 Hybri-Max (Sigma-Aldrich) density centrifugation in Leucosep tubes (Greiner). The human Pan Monocyte Isolation Kit (Miltenyi Biotec) was used to isolate monocytes from PBMCs. This study was approved by the research ethics committee (UK multicentre ethics approval REC 07/H0718/49) and abides by the principles of the Declaration of Helsinki.

Flow cytometry

Experiments were carried out using HEPES binding buffer (10 mM HEPES, 140 mM NaCl, 2.5 mM $CaCl_2$, pH 7.4), supplemented with 2% BSA after viability staining. Cells were stained with LIVE/DEAD Fixable Near-IR Dead Cell Stain (Thermo Fisher Scientific). PBMCs were Fc receptor blocked with Human TruStain FcX (BioLegend) and then surface stained with anti-CD3 PerCP-Cy5.5 (OKT3), anti-CD4 FITC (OKT4), anti-CD8a BV421 (RPA-T8), anti-CD19 BV421 (HIB19), anti-CD14 FITC (M5E2), anti-CD14 PerCP-Cy5.5 (HCD14), or anti-CD16 APC (3G8, all BioLegend) in panels as appropriate, with 1:25 anti-nucleolin PE (H-6) and IgG2a PE isotype control (both Santa Cruz Biotechnologies) or 5 μM GFP-C1QTNF4 and GFP A206K for 40 min on ice protected from light. PBMCs were fixed in 4% formaldehyde (Thermo Fisher Scientific) for 20 min on ice. For binding assays, cells were incubated with GFP-C1QTNF4 for 1 h on ice. For competition assays, nucleolin constructs R1234G, R123, and R4G, LPS from *E. coli* O111:B4 (Sigma-Aldrich), human recombinant iron-saturated lactoferrin (Sigma-Aldrich) or the DNA aptamer AS1411 (5'-GGTGGTGGTGGTTGTGGTGGTGGTGG-3', Integrated DNA Technologies) were added prior to GFP-C1QTNF4 and incubated together for 1 h on ice. Cell-binding data were acquired on a BD FACSCanto II or BD LSRFortessa using BD FACSDiva Software v8.0.1 (all BD Biosciences), where compensation was also performed. Data were analyzed in FlowJo Software v10 (BD Biosciences) and median fluorescence intensity (MFI) was calculated. Visualization of MFI, curve fitting, as well as calculation of maximum binding (plateau) and half-maximal effective concentration (EC_{50}) by nonlinear regression were performed in Prism 8 (GraphPad).

Apoptosis induction and annexin staining

Jurkat T cells were cultured at 5×10^5 cells/ml in RPMI-1640 medium containing 2 mM L-glutamine, 10% heat-inactivated FBS, 100 U/ml penicillin, and 100 μg/ml streptomycin supplemented with 1 μM staurosporine (Cell Guidance Systems) for 4 h at 37 °C and 5% CO_2 to induce apoptosis. After GFP-C1QTNF4 binding, staining with Annexin V APC in 1X binding buffer (Thermo Fisher Scientific) was performed for 10 min at room temperature protected from light. Samples were washed and resuspended in 1X binding buffer for data acquisition by flow cytometry.

Imaging flow cytometry

PBMCs were incubated in 1.25 μM GFP-C1QTNF4 in RPMI-1640 medium containing 2 mM L-glutamine, 10% heat-inactivated FBS, 100 U/ml penicillin, and 100 μg/ml streptomycin for 30 min on ice or at 37 °C and 5% CO_2. Washes in-between steps were carried out with Dulbecco's PBS containing 2% BSA and 2 mM EDTA. Cells were Fc receptor blocked with Human TruStain FcX and stained with anti-CD14 PerCP-Cy5.5 (HCD14) for 20 min on ice. Fixation was performed with BD Cytofix Fixation Buffer (BD Biosciences) for 20 min on ice. Cells were permeabilized with 0.1% Triton X-100 (Sigma-Aldrich) for 30 min on ice to facilitate staining with 1.8 μM DAPI (BioLegend) prior to acquisition. Cells were acquired on an Amnis ImageStream^X Mk II imaging flow cytometer using INSPIRE software. Compensation and analysis were performed in IDEAS software v6.1 (all Luminex). The Internalization feature was used to compare internalization at 37 °C *versus* incubation on ice, with images of approximately 10,000 CD14+ monocytes used for analysis.

Microscopy

HEK293 cells were seeded onto coverslips coated with poly-L-lysine (Sigma-Aldrich). Cells were incubated in 2.5 μM GFP-C1QTNF4 in complete medium for 1.5 h on ice or at 37 °C and 5% CO_2, then rested in complete medium for a further 0.5 h. Cells were fixed in 4% formaldehyde for 20 min, permeabilized with 0.1% Triton X-100 for 15 min, and counterstained with 600 nM DAPI for 5 min at room temperature. Coverslips were mounted in ProLong Glass Antifade Mountant (Thermo Fisher Scientific). Images were acquired using an Axioplan2 microscope (Zeiss) with a 40×/0.75 objective, fitted with an Infinity 3 camera, and data acquisition was managed in Infinity Analyze v6.5.4 (both Lumenera). Image processing was performed using Icy image analysis software v1.9.9.1.

SEC-MALLS

SEC-MALLS was performed using a Superdex 200 Increase 5/150 GL column (Cytiva) at a flow rate of 0.3 ml/min using a miniDAWN light-scattering detector and an Optilab DSP Interferometric Refractometer (both Wyatt Technology) at room temperature. Samples were injected at a volume of 50 µl and at the following concentrations: C1QTNF4-d1 at 3 mg/ml, GFP A206K at 2 mg/ml, GFP-d1 at 1.1 mg/ml, GFP-d2 at 1.3 mg/ml and GFP-C1QTNF4 at 1.1 mg/ml in 50 mM Tris, 150 mM NaCl, 4 mM $CaCl_2$, 0.1% NaN_3, pH 7.4; C1QTNF4 at 1.4 mg/ml in 50 mM Tris, 500 mM NaCl, 4 mM $CaCl_2$, 0.1% NaN_3, pH 8.55. The data were collected and analyzed using the ASTRA 4.9 software (Wyatt Technology). The data for refractive index and molecular mass were visualized by plotting in Prism 8 (GraphPad).

Statistical analysis

Statistical analysis was performed in Prism 8 (GraphPad). An unpaired *t*-test or an ordinary one-way ANOVA with Tukey's multiple comparisons test was performed as indicated.

Data availability

The mass spectrometry proteomics data have been deposited to the ProteomeXchange Consortium *via* the PRIDE partner repository (67) with the data set identifier PXD023088 and are accessible at https://www.ebi.ac.uk/pride/.

Supporting information—This article contains supporting information.

Acknowledgments—We thank Professor Andrew Cope (King's College London) for helpful suggestions.

Author contributions—S. K. V., R. L. B., S. L., and A. J. B.: investigation; S. K. V. and S. L.: formal analysis; S. K. V.: visualization; R. L. B., S. L., A. J. B., and T. J. V.: resources; S. K. V., R. L. B., D. S. C. G., J. M. M., and T. J. V.: conceptualization; R. L. B., D. S. C. G., J. M. M., and T. J. V.: supervision; S. K. V., D. S. C. G., and T. J. V.: funding acquisition; S. K. V.: writing—original draft; S. K. V., R. L. B., S. L., A. J. B., D. S. C. G., J. M. M., and T. J. V.: writing—review and editing.

Funding and additional information—This work was primarily funded by Versus Arthritis PhD studentship 21252 (to S. K. V., D. S. C. G., and T. J. V.). This research was supported by the National Institute for Health Research (NIHR) Biomedical Research Centre based at Guy's and St Thomas' NHS Foundation Trust and King's College London (to T. J. V.). The views expressed are those of the authors and not necessarily those of the NHS, the NIHR, or the Department of Health and Social Care. We acknowledge financial support through the NIHR-funded BRC Flow Cytometry Core at Guy's and St Thomas' NHS Foundation Trust in partnership with King's College London.

Conflict of interest—The authors declare that they have no conflicts of interest with the contents of this article.

Abbreviations—The abbreviations used are: C1QTNF4, C1q and TNF related 4; co-IP, co-immunoprecipitation; FBS, fetal bovine serum; GAR, glycine/arginine rich; IL-6, interleukin 6; LC-MS/MS, liquid chromatography–tandem mass spectrometry; LPS, lipopolysaccharide; MFI, median fluorescence intensity; PBMCs, peripheral blood mononuclear cells; R1-4, RNA-binding domains 1–4; RSV, respiratory syncytial virus; SEC-MALLS, size-exclusion chromatography with multiangle laser light scattering; SLE, systemic lupus erythematosus; TLR, toll-like receptor; TNF, tumor necrosis factor.

References

1. Wong, G. W., Wang, J., Hug, C., Tsao, T.-S., and Lodish, H. F. (2004) A family of Acrp30/adiponectin structural and functional paralogs. *Proc. Natl. Acad. Sci. U. S. A.* **101**, 10302–10307
2. Shapiro, L., and Scherer, P. E. (1998) The crystal structure of a complement-1q family protein suggests an evolutionary link to tumor necrosis factor. *Curr. Biol.* **8**, 335–338
3. Li, Q., Wang, L., Tan, W., Peng, Z., Luo, Y., Zhang, Y., Zhang, G., Na, D., Jin, P., Shi, T., Ma, D., and Wang, L. (2011) Identification of C1qTNF-related protein 4 as a potential cytokine that stimulates the STAT3 and NF-κB pathways and promotes cell survival in human cancer cells. *Cancer Lett.* **308**, 203–214
4. Luo, Y., Wu, X., Ma, Z., Tan, W., Weng, L., Na, D., Zhang, G., Yin, A., Huang, H., Xia, D., Zhang, Y., Shi, X., and Wang, L. (2016) Expression of the novel adipokine C1qTNF-related protein 4 (CTRP4) suppresses colitis and colitis-associated colorectal cancer in mice. *Cell. Mol. Immunol.* **13**, 688–699
5. Xu, W., Zhou, H., Li, X., Wang, L., Guo, X., Yin, L., Chang, H., Wei, Y., Li, Q., Deng, J., Zhou, X., Yang, H., Zhang, X., Yi, F., and Ma, W. (2019) C1Q/TNF-related protein 4 expression correlates with herpes simplex encephalitis progression. *Ann. Transl. Med.* **7**, 235
6. Byerly, M. S., Petersen, P. S., Ramamurthy, S., Seldin, M. M., Lei, X., Provost, E., Wei, Z., Ronnett, G. V., and Wong, G. W. (2014) C1q/TNF-related protein 4 (CTRP4) is a unique secreted protein with two tandem C1q domains that functions in the hypothalamus to modulate food intake and body weight. *J. Biol. Chem.* **289**, 4055–4069
7. Li, Y., Ye, L., Jia, G., Chen, H., Yu, L., and Wu, D. (2020) C1q/TNF-related protein 4 induces signal transducer and activator of transcription 3 pathway and modulates food intake. *Neuroscience* **429**, 1–9
8. Sarver, D. C., Stewart, A. N., Rodriguez, S., Little, H. C., Aja, S., and Wong, G. W. (2020) Loss of CTRP4 alters adiposity and food intake behaviors in obese mice. *Am. J. Physiol. Endocrinol. Metab.* **319**, E1084–E1100
9. Tsokos, G. C., Lo, M. S., Reis, P. C., and Sullivan, K. E. (2016) New insights into the immunopathogenesis of systemic lupus erythematosus. *Nat. Rev. Rheumatol.* **12**, 716–730
10. Pullabhatla, V., Roberts, A. L., Lewis, M. J., Mauro, D., Morris, D. L., Odhams, C. A., Tombleson, P., Liljedahl, U., Vyse, S., Simpson, M. A., Sauer, S., de Rinaldis, E., Syvänen, A.-C., and Vyse, T. J. (2018) De novo mutations implicate novel genes in systemic lupus erythematosus. *Hum. Mol. Genet.* **27**, 421–429
11. Pakzad, B., Shirpour, R., Mousavi, M., Karimzadeh, H., Salehi, A., Kazemi, M., Amini, G., Akbari, M., and Salehi, R. (2020) C1QTNF4 gene p.His198Gln mutation is correlated with early-onset systemic lupus erythematosus in Iranian patients. *Int. J. Rheum. Dis.* **23**, 1594–1598
12. Hovanessian, A. G., Soundaramourty, C., El Khoury, D., Nondier, I., Svab, J., and Krust, B. (2010) Surface expressed nucleolin is constantly induced in tumor cells to mediate calcium-dependent ligand internalization. *PLoS One* **5**, e15787
13. Christian, S., Pilch, J., Akerman, M. E., Porkka, K., Laakkonen, P., and Ruoslahti, E. (2003) Nucleolin expressed at the cell surface is a marker of endothelial cells in angiogenic blood vessels. *J. Cell Biol.* **163**, 871–878
14. Hirano, K., Miki, Y., Hirai, Y., Sato, R., Itoh, T., Hayashi, A., Yamanaka, M., Eda, S., and Beppu, M. (2005) A multifunctional shuttling protein nucleolin is a macrophage receptor for apoptotic cells. *J. Biol. Chem.* **280**, 39284–39293
15. Wise, J. F., Berkova, Z., Mathur, R., Zhu, H., Braun, F. K., Tao, R. H., Sabichi, A. L., Ao, X., Maeng, H., and Samaniego, F. (2013) Nucleolin

inhibits Fas ligand binding and suppresses Fas-mediated apoptosis *in vivo* via a surface nucleolin-Fas complex. *Blood* **121**, 4729–4739
16. Legrand, D., Vigié, K., Said, E. A., Elass, E., Masson, M., Slomianny, M. C., Carpentier, M., Briand, J. P., Mazurier, J., and Hovanessian, A. G. (2004) Surface nucleolin participates in both the binding and endocytosis of lactoferrin in target cells. *Eur. J. Biochem.* **271**, 303–317
17. Take, M., Tsutsui, J., Obama, H., Ozawa, M., Nakayama, T., Maruyama, I., Arima, T., and Muramatsu, T. (1994) Identification of nucleolin as a binding protein for midkine (MK) and heparin-binding growth associated molecule (HB-GAM). *J. Biochem.* **116**, 1063–1068
18. Wang, Y., Mao, M., and Xu, J. (2011) Cell-surface nucleolin is involved in lipopolysaccharide internalization and signalling in alveolar macrophages. *Cell Biol. Int.* **35**, 677–685
19. Tayyari, F., Marchant, D., Moraes, T. J., Duan, W., Mastrangelo, P., and Hegele, R. G. (2011) Identification of nucleolin as a cellular receptor for human respiratory syncytial virus. *Nat. Med.* **17**, 1132–1135
20. Warrener, P., and Petryshyn, R. (1991) Phosphorylation and proteolytic degradation of nucleolin from 3T3-F442A cells. *Biochem. Biophys. Res. Commun.* **180**, 716–723
21. Fang, S.-H., and Yeh, N.-H. (1993) The self-cleaving activity of nucleolin determines its molecular dynamics in relation to cell proliferation. *Exp. Cell Res.* **208**, 48–53
22. Bates, P. J., Laber, D. A., Miller, D. M., Thomas, S. D., and Trent, J. O. (2009) Discovery and development of the G-rich oligonucleotide AS1411 as a novel treatment for cancer. *Exp. Mol. Pathol.* **86**, 151–164
23. Phillips, G. N. (1997) Structure and dynamics of green fluorescent protein. *Curr. Opin. Struct. Biol.* **7**, 821–827
24. Zacharias, D. A., Violin, J. D., Newton, A. C., and Tsien, R. Y. (2002) Partitioning of lipid-modified monomeric GFPs into membrane microdomains of live cells. *Science* **296**, 913–916
25. Wong, G. W., Krawczyk, S. A., Kitidis-Mitrokostas, C., Revett, T., Gimeno, R., and Lodish, H. F. (2008) Molecular, biochemical and functional characterizations of C1q/TNF family members: Adipose-tissue-selective expression patterns, regulation by PPAR-γ agonist, cysteine-mediated oligomerizations, combinatorial associations and metabolic functions. *Biochem. J.* **416**, 161–177
26. Neumeier, M., Weigert, J., Schäffler, A., Wehrwein, G., Müller-Ladner, U., Schölmerich, J., Wrede, C., and Buechler, C. (2006) Different effects of adiponectin isoforms in human monocytic cells. *J. Leukoc. Biol.* **79**, 803–808
27. Song, H., Chan, J., and Rovin, B. H. (2009) Induction of chemokine expression by adiponectin *in vitro* is isoform dependent. *Transl. Res.* **154**, 18–26
28. Nagata, S., Hanayama, R., and Kawane, K. (2010) Autoimmunity and the clearance of dead cells. *Cell* **140**, 619–630
29. Korb, L. C., and Ahearn, J. M. (1997) C1q binds directly and specifically to surface blebs of apoptotic human keratinocytes: Complement deficiency and systemic lupus erythematosus revisited. *J. Immunol.* **158**, 4525–4528
30. Navratil, J. S., Watkins, S. C., Wisnieski, J. J., and Ahearn, J. M. (2001) The globular heads of C1q specifically recognize surface blebs of apoptotic vascular endothelial cells. *J. Immunol.* **166**, 3231–3239
31. Ogden, C. A., DeCathelineau, A., Hoffmann, P. R., Bratton, D., Ghebrehiwet, V. A., Fadok, B., and Henson, P. M. (2001) C1q and mannose binding lectin engagement of cell surface calreticulin and CD91 initiates macropinocytosis and uptake of apoptotic cells. *J. Exp. Med.* **194**, 781–795
32. Said, E. A., Krust, B., Nisole, S., Svab, J., Briand, J. P., and Hovanessian, A. G. (2002) The anti-HIV cytokine midkine binds the cell surface-expressed nucleolin as a low affinity receptor. *J. Biol. Chem.* **277**, 37492–37502
33. Said, E. A., Courty, J., Svab, J., Delbé, J., Krust, B., and Hovanessian, A. G. (2005) Pleiotrophin inhibits HIV infection by binding the cell surface-expressed nucleolin. *FEBS J.* **272**, 4646–4659
34. Allen, K. L., Fonseca, F. V., Betapudi, V., Willard, B., Zhang, J., and McCrae, K. R. (2012) A novel pathway for human endothelial cell activation by antiphospholipid/anti-β 2 glycoprotein I antibodies. *Blood* **119**, 884–893
35. Pradeep, A. N., Asea, A., and Kaur, P. (2016) Nucleolin transports Hsp72 to the plasma membrane preparatory to its release into the microenvironment. *J. Cell Sci. Ther.* **7**, 1000254
36. Yuan, X., Hu, T., He, H., Qiu, H., Wu, X., Chen, J., Wang, M., Chen, C., and Huang, S. (2018) Respiratory syncytial virus prolifically infects N2a neuronal cells, leading to TLR4 and nucleolin protein modulations and RSV F protein co-localization with TLR4 and nucleolin. *J. Biomed. Sci.* **25**, 13
37. Hu, T., Yu, H., Lu, M., Yuan, X., Wu, X., Qiu, H., Chen, J., and Huang, S. (2019) TLR4 and nucleolin influence cell injury, apoptosis and inflammatory factor expression in respiratory syncytial virus-infected N2a neuronal cells. *J. Cell. Biochem.* **120**, 16206–16218
38. Akashi, S., Saitoh, S., Wakabayashi, Y., Kikuchi, T., Takamura, N., Nagai, Y., Kusumoto, Y., Fukase, K., Kusumoto, S., Adachi, Y., Kosugi, A., and Miyake, K. (2003) Lipopolysaccharide interaction with cell surface toll-like receptor 4-MD-2: Higher affinity than that with MD-2 or CD14. *J. Exp. Med.* **198**, 1035–1042
39. Kurt-Jones, E. A., Popova, L., Kwinn, L., Haynes, L. M., Jones, L. P., Tripp, R. A., Walsh, E. E., Freeman, M. W., Golenbock, D. T., Anderson, L. J., and Finberg, R. W. (2000) Pattern recognition receptors TLR4 and CD14 mediate response to respiratory syncytial virus. *Nat. Immunol.* **1**, 398–401
40. Schilling, D., Thomas, K., Nixdorff, K., Vogel, S. N., and Fenton, M. J. (2002) Toll-like receptor 4 and toll-IL-1 receptor domain-containing adapter protein (TIRAP)/myeloid differentiation protein 88 adapter-like (mal) contribute to maximal IL-6 expression in macrophages. *J. Immunol.* **169**, 5874–5880
41. Ando, K., Hasegawa, K., Shindo, K., Furusawa, T., Fujino, T., Kikugawa, K., Nakano, H., Takeuchi, O., Akira, S., Akiyama, T., Gohda, J., Inoue, J., and Hayakawa, M. (2010) Human lactoferrin activates NF-κB through the toll-like receptor 4 pathway while it interferes with the lipopolysaccharide-stimulated TLR4 signaling. *FEBS J.* **277**, 2051–2066
42. Cao, L., Tan, W., Chen, W., Huang, H., He, M., Li, Q., Zhu, X., and Wang, L. (2021) CTRP4 acts as an anti-inflammatory factor in macrophages and protects against endotoxic shock. *Eur. J. Immunol.* **51**, 380–392
43. Kopp, A., Bala, M., Buechler, C., Falk, W., Gross, P., Neumeier, M., Schölmerich, J., and Schäffler, A. (2010) C1q/TNF-related protein-3 represents a novel and endogenous lipopolysaccharide antagonist of the adipose tissue. *Endocrinology* **151**, 5267–5278
44. Liu, M., Yin, L., Li, W., Hu, J., Wang, H., Ye, B., Tang, Y., and Huang, C. (2019) C1q/TNF-related protein-9 promotes macrophage polarization and improves cardiac dysfunction after myocardial infarction. *J. Cell. Physiol.* **234**, 18731–18747
45. Husebye, H., Halaas, Ø., Stenmark, H., Tunheim, G., Sandanger, Ø., Bogen, B., Brech, A., Latz, E., and Espevik, T. (2006) Endocytic pathways regulate toll-like receptor 4 signaling and link innate and adaptive immunity. *EMBO J.* **25**, 683–692
46. Feng, S., Su, Y., Luo, L., Jing, F., and Yi, Q. (2018) Serum levels of C1q/tumor necrosis factor-related protein-1 in children with Kawasaki disease. *Pediatr. Res.* **83**, 999–1003
47. Murayama, M. A., Kakuta, S., Maruhashi, T., Shimizu, K., Seno, A., Kubo, S., Sato, N., Saijo, S., Hattori, M., and Iwakura, Y. (2014) CTRP3 plays an important role in the development of collagen-induced arthritis in mice. *Biochem. Biophys. Res. Commun.* **443**, 42–48
48. Cooper, J. D., Smyth, D. J., Smiles, A. M., Plagnol, V., Walker, N. M., Allen, J. E., Downes, K., Barrett, J. C., Healy, B. C., Mychaleckyj, J. C., Warram, J. H., and Todd, J. A. (2008) Meta-analysis of genome-wide association study data identifies additional type 1 diabetes risk loci. *Nat. Genet.* **40**, 1399–1401
49. Onengut-Gumuscu, S., Chen, W.-M., Burren, O., Cooper, N. J., Quinlan, A. R., Mychaleckyj, J. C., Farber, E., Bonnie, J. K., Szpak, M., Schofield, E., Achuthan, P., Guo, H., Fortune, M. D., Stevens, H., Walker, N. M., *et al.* (2015) Fine mapping of type 1 diabetes susceptibility loci and evidence for colocalization of causal variants with lymphoid gene enhancers. *Nat. Genet.* **47**, 381–386
50. Julià, A., Ballina, J., Cañete, J. D., Balsa, A., Tornero-Molina, J., Naranjo, A., Alperi-López, M., Erra, A., Pascual-Salcedo, D., Barcelò, P., Camps, J., and Marsal, S. (2008) Genome-wide association study of rheumatoid arthritis in the Spanish population: KLF12 as a risk locus for rheumatoid arthritis susceptibility. *Arthritis Rheum.* **58**, 2275–2286
51. Murayama, M. A., Kakuta, S., Inoue, A., Umeda, N., Yonezawa, T., Maruhashi, T., Tateishi, K., Ishigame, H., Yabe, R., Ikeda, S., Seno, A.,

Chi, H. H., Hashiguchi, Y., Kurata, R., Tada, T., *et al.* (2015) CTRP6 is an endogenous complement regulator that can effectively treat induced arthritis. *Nat. Commun.* **6**, 8483
52. Langefeld, C. D., Ainsworth, H. C., Cunninghame Graham, D. S., Kelly, J. A., Comeau, M. E., Harley, J. B., Wakeland, E. K., Graham, R. R., Gaffney, P. M., and Vyse, T. J. (2017) Transancestral mapping and genetic load in systemic lupus erythematosus. *Nat. Commun.* **8**, 16021
53. Lonsdale, J., Thomas, J., Salvatore, M., Phillips, R., Lo, E., Shad, S., Hasz, R., Walters, G., Garcia, F., Young, N., Foster, B., Moser, M., Karasik, E., Gillard, B., Ramsey, K., *et al.* (2013) The genotype-tissue expression (GTEx) project. *Nat. Genet.* **45**, 580–585
54. Wu, C., Orozco, C., Boyer, J., Leglise, M., Goodale, J., Batalov, S., Hodge, C. L., Haase, J., Janes, J., Huss, J. W., III, and Su, A. I. (2009) BioGPS: An extensible and customizable portal for querying and organizing gene annotation resources. *Genome Biol.* **10**, R130
55. McCall, M. N., Uppal, K., Jaffee, H. A., Zilliox, M. J., and Irizarry, R. A. (2011) The gene expression barcode: Leveraging public data repositories to begin cataloging the human and murine transcriptomes. *Nucleic Acids Res.* **39**, D1011–D1015
56. Mabbott, N. A., Baillie, J. K., Brown, H., Freeman, T. C., and Hume, D. A. (2013) An expression atlas of human primary cells: Inference of gene function from coexpression networks. *BMC Genomics* **14**, 632
57. Huang, T.-S., Hsieh, J.-Y., Wu, Y.-H., Jen, C.-H., Tsuang, Y.-H., Chiou, S.-H., Partanen, J., Anderson, H., Jaatinen, T., Yu, Y.-H., and Wang, H.-W. (2008) Functional network reconstruction reveals somatic stemness genetic maps and dedifferentiation-like transcriptome reprogramming induced by GATA2. *Stem Cells* **26**, 1186–1201
58. Monaco, G., Lee, B., Xu, W., Mustafah, S., Hwang, Y. Y., Carré, C., Burdin, N., Visan, L., Ceccarelli, M., Poidinger, M., Zippelius, A., Pedro de Magalhães, J., and Larbi, A. (2019) RNA-seq signatures normalized by mRNA abundance allow absolute deconvolution of human immune cell types. *Cell Rep.* **26**, 1627–1640
59. Okamura, Y., Aoki, Y., Obayashi, T., Tadaka, S., Ito, S., Narise, T., and Kinoshita, K. (2015) COXPRESdb in 2015: Coexpression database for animal species by DNA-microarray and RNAseq-based expression data with multiple quality assessment systems. *Nucleic Acids Res.* **43**, D82–D86
60. Terskikh, A. V., Easterday, M. C., Li, L., Hood, L., Kornblum, H. I., Geschwind, D. H., and Weissman, I. L. (2001) From hematopoiesis to neuropoiesis: Evidence of overlapping genetic programs. *Proc. Natl. Acad. Sci. U. S. A.* **98**, 7934–7939
61. Grinstein, E., Du, Y., Santourlidis, S., Christ, J., Uhrberg, M., and Wernet, P. (2007) Nucleolin regulates gene expression in CD34-positive hematopoietic cells. *J. Biol. Chem.* **282**, 12439–12449
62. Mahotka, C., Bhatia, S., Kollet, J., and Grinstein, E. (2018) Nucleolin promotes execution of the hematopoietic stem cell gene expression program. *Leukemia* **32**, 1865–1868
63. Omeka, W. K. M., Liyanage, D. S., Priyathilaka, T. T., Kwon, H., Lee, S., and Lee, J. (2019) Characterization of four C1q/TNF-related proteins (CTRPs) from red-lip mullet (Liza haematocheila) and their transcriptional modulation in response to bacterial and pathogen-associated molecular pattern stimuli. *Fish Shellfish Immunol.* **84**, 158–168
64. Klock, H. E., and Lesley, S. A. (2009) The polymerase incomplete primer extension (PIPE) method applied to high-throughput cloning and site-directed mutagenesis. In *High Throughput Protein Expression and Purification. Methods in Molecular Biology*, Vol 498, Humana Press, Totowa, NJ: 91–103
65. Studier, F. W. (2005) Protein production by auto-induction in high-density shaking cultures. *Protein Expr. Purif.* **41**, 207–234
66. Eng, J. K., McCormack, A. L., and Yates, J. R. (1994) An approach to correlate tandem mass spectral data of peptides with amino acid sequences in a protein database. *J. Am. Soc. Mass Spectrom.* **5**, 976–989
67. Perez-Riverol, Y., Csordas, A., Bai, J., Bernal-Llinares, M., Hewapathirana, S., Kundu, D. J., Inuganti, A., Griss, J., Mayer, G., Eisenacher, M., Pérez, E., Uszkoreit, J., Pfeuffer, J., Sachsenberg, T., Yılmaz, Ş., *et al.* (2019) The PRIDE database and related tools and resources in 2019: Improving support for quantification data. *Nucleic Acids Res.* **47**, D442–D450